Computerized Medical Imaging and Graphics, Vol. 17, No. 3, pp. 189–200, 1993
Printed in the U.S.A.

0895-6111/93 $6.00 + .00

METHOD FOR 3D VOLUMETRIC ANALYSIS OF INTRANUCLEAR FLUORESCENCE DISTRIBUTION IN CONFOCAL MICROSCOPY

Franck Parazza*, Catherine Humbert, and Yves Usson
Equipe de Reconnaissance des Formes et Microscopie Quantitative, Laboratoire TIM3-IMAG, USR CNRS 690B, CERMO, Université Joseph Fourier, BP 53X 38041 Grenoble Cedex, France

(Received 21 October 1992)

Abstract—The introduction of the confocal laser scanning microscope makes it possible to acquire fluorescent specimens in 3D. We present basic image processing tools to enhance the data and to quantitate the morphology and topography of the intravolume elements. The tools were applied to the description of the spatial distribution of DNA replication sites in mammalian cell nuclei as an example.

Key Words: 3D analysis, Image processing, Confocal microscopy, DNA replication

INTRODUCTION

In the field of cellular biology, many two-dimensional (2D) quantitative studies are made using conventional optical microscopy and computerized image analysis. Although these studies generally lead to interesting results, it is sometimes impossible to retrieve and describe three-dimensional (3D) structures from 2D data. Three-dimensional data acquisition has become feasible with the development of the confocal laser scanning microscope (CLSM). Until recently, much effort has been expended to generate methods for the display of 3D data on a 2D screen (1, 2). These methods have been helpful to understand complex structures and to describe biological specimens qualitatively (3). However, as is the case with the 2D approach, there is a need for a quantitative approach to avoid visual subjectivity.

The aim of this paper was to propose a method for the quantitative description of the 3D spatial distribution of events inside near-convex volumes acquired by fluorescence CLSM. Methods for 3D quantitative analysis have been developed in the medical field and for electron microscopy (4, 5). Therefore, instead of introducing new tools, we selected and adapted existing ones to answer our specific problems. The choice of the different computer methods was based on the needs and the constraints in cellular biology. For this reason, the processing time was one of the main considerations for the choice of specific tools. We describe two groups of tools: preprocessing and "processing." Preprocessing is used to restore and enhance the volume data. Processing is used to extract the significant objects from the volume, and to compute intravolume distances and other features in order to quantitate spatial information. We applied them to the description of the spatial distribution of DNA replication sites in mammalian cell nuclei as an example.

* Correspondence should be addressed to Franck Parazza, Equipe de Reconnaissance des formés et Microscopie Quantitative, Laboratoire TIM3-IMAG, USR CNRS 690B, CERMO, Université Joseph Fourier, BP 53X 38041 Grenoble Cedex, France.

MATERIALS AND METHODS

Data acquisition

A Zeiss CLSM LSM10 fitted with a double photodetector was used for data acquisition (courtesy of Zeiss, France). In order to ensure high resolution, an objective with a high numerical aperture was used (×63, NA 1.4, Plan-apochromat oil immersion). With this setting, the resolution of the optical system of the CLSM was about 0.2 μm in the focal plane and about 0.7 μm in the axial direction. The CLSM makes it possible to acquire digitized optical sections from a transparent fluorescent specimen. The data are a stack of 2D digitized sections. They may be also described as a 3D array of volume elements (voxel), in which the value of a voxel is proportional to the fluorescence intensity in a subvolume of the specimen. The values range from 0 to 255 (8 bit words). The sampling step for digitation was 0.14 μm in the focal plane and 0.294 μm along the optical axis. Consequently, the discrete volume is composed of noncubic voxels. In the volume space, each voxel, V, is indexed by the following discrete coordinates:

$$i \in [0, I_{max}[, j \in [0, J_{max}[\text{ and } k \in [0, K_{max}[.$$

In the actual space, the dimensions of the voxels are defined by the sampling steps S_i, S_j, and S_k used during

the acquisition process. In our application, typical values were 256 for I_{max} and J_{max} and 40 for K_{max}; S_i and S_j were 0.14 μm and S_k was 0.29 μm.

Computer equipment

The analysis of this large data set requires the use of a fast and efficient computer with a large RAM memory. A Silicon Graphics Indigo™ workstation (RISC processor, 30 MIPS) fitted with 32 megabytes of RAM was used. The programmes were written in standard C language and the display interface was based on the GL library (Silicon Graphics) and the FORMS user interface (Mark Overmars, Department of Computer Science, Utrecht University, the Netherlands).

Preprocessing

Once a discrete volume had been acquired, it was necessary to correct for the artefacts generated by the acquisition system. Three main image artefacts were taken into account: (i) high noise level; (ii) out of focus blur; and (iii) noncubic shape of the voxels. All these artefacts must be corrected before beginning a quantitative analysis. Different algorithms to remove these artefacts are available (6–8). Although some of these may reach a very high efficiency, their use in a cell biological application is compromized by lengthy computing times.

Noise reduction. The CLSM generates digital sections with a poor signal to noise ratio (when no trade off between the axial resolution and the signal to noise ratio is permitted). The main source of noise is the electronics of the CLSM. A 3D median filter was used to remove this noise. This filter has the property of removing noise spikes while maintaining the main edge information in the data set. The median filter is used to remove the voxels whose values are inconsistent with their surrounding values. A $3 \times 3 \times 3$ box is centred over each voxel of the discrete volume. The filter sorts the voxels within the box in the source volume and replaces the centred voxel value with the median value in the destination volume. In our implementation of the median filter, the surrounding voxels were those that share a face with the current voxel (the 6-connected voxels).

Blur removal. The pin-hole increases the axial resolution of the CLSM by reducing the out-of-focus information in the acquired sections. However, a residual contamination of the out-of-focus sections still remains. The purpose of this step is to remove the out-of-focus information. Therefore, it is necessary to evaluate how the imperfection of the optical system blurs the sections. The theoretical description of the blur is called the point spread function (PSF) of the optical system. This function can be obtained experimentally by recording the blur induced on images of subresolution fluorescent beads (9). When the PSF is known, it should be possible to remove the out of focus information that contaminates each digitized section. Four main methods have been described in the literature: the iterative deconvolution (10), the regularization method (11), the maximum likelihood (12), and the nearest neighbors (13). Although the first three methods provide a very good restoration, their lengthy computing times are not compatible with a practical use in biological applications. The fourth method offers an acceptable compromise between speed and restoration efficiency. Consequently, an algorithm based on this method was used to deblur our discrete volumes.

The nearest neighbors method is the simplest scheme for debluring (13). Only the information of the single section above and the single section below is actually needed, because contamination from adjacent sections contributes most strongly in the bluring of the central section. Let V be the acquired discrete volume, T the actual corresponding volume in the biological specimen and h the PSF:

$$V_j = T_j \otimes h_0 + T_{j+1} \otimes h_1 + T_{j-1} \otimes h_{-1} + \epsilon,$$

where $\otimes$ denotes a 2D convolution and ϵ the neglected contribution of the other planes. The subscripts on V and T refer to the section indices. The subscript on h refers to the number of interplane spacings away from the focus. Assuming that T_{j+1} is nearly identical to V_{j+1} and that h_1 is nearly identical h_{-1} an approximation of T_j can be calculated:

$$T_j = (V_j - C(V_{j+1} + V_{j-1}) \otimes h_1) \otimes h_0^{-1}.$$

If the in-focus PSF h_0 is neglected (no lateral resolution improvement), the out-of-focus section contamination removal can be expressed as:

$$V'_j = V_j - C(V_{j+1} + V_{j-1}) \otimes h_1.$$

The result of this debluring is an improvement of the axial resolution. The coefficient of "contamination" C was empirically set to 0.33 in our case.

Interpolation. The data acquisition conditions lead to a 3D array of noncubic voxels. This noncubic shape is not compatible with the use of morphological operators based on distance transforms (i.e., shrinking, expanding, opening and closing) required in further stages of the processing step. Because these operations require an isotropic propagation medium to work properly, the geometry of the voxels must be transformed. Therefore, interleveled sections were interpolated from the original discrete volume. The interpolated sections can be derived from the adjacent

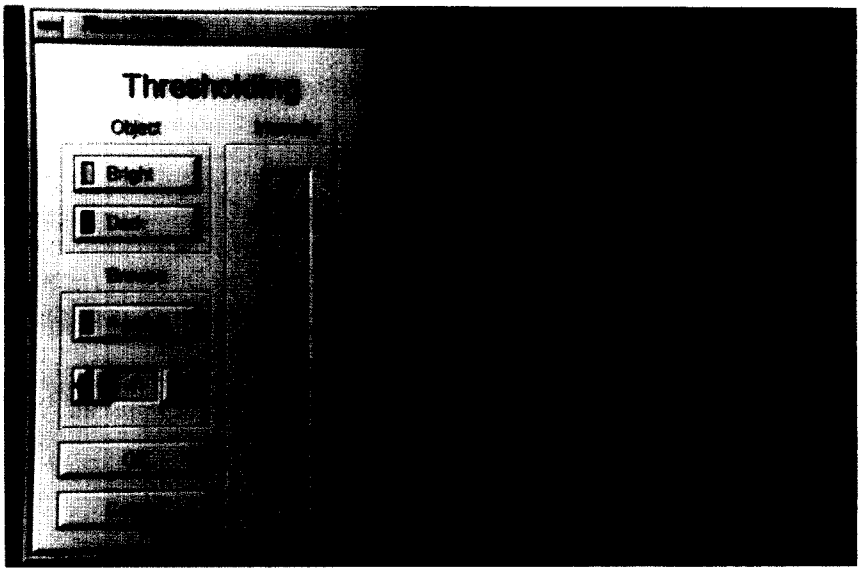

Fig. 1. Discrete volume segmentation. The discrete volume is segmented interactively using a graphic interface. The segmentation result can be displayed for the entire volume on orthogonal cross sections (*xy*, *yz*, *xz*). The choice of each section is made by moving the cross in the *xy* window. The threshold value is chosen by the use of a scroll bar in the dialogue box.

sections by B-spline interpolation or bi-linear interpolation (14). Although the property of double derivation of B-spline curves leads to a smoother result than bi-linear interpolation, the drawback of B-spline curves is the time to compute the spline coefficients. Therefore, the bi-linear approach was chosen.

Let V be the discrete volume, ci the ratio between the axial size Sk and the lateral size Si or Sj of a voxel. K_{max} is the number of the original sections, K'_{max} the number of interpolated sections and V_{new} is the interpolated discrete volume. $Ent(X)$ returns the integer part of X.

$K'_{max} = K_{max}\ ci$; $k = 0$;
FOR $k' = 0$ TO K'_{max} DO
  $k = \text{Ent}(k'/ci)$; $d = (k'/ci) - Ent(k'/ci)$;
  FOR $j = 0$ to J_{max} do
    FOR $i = 0$ to I_{max} do
      $V_{new}(i, j, k') = d\ V(i, j, k) + (1 - d)\ V(i, j, k + 1)$;
    END FOR
  END FOR
END FOR

Processing

After the preprocessing step, we assume that the main artifacts have been removed from the discrete volume. Although the processing step is dedicated to a specific application, there are general points in the way to proceed. As in the 2D domain, the objects need to be first extracted from the scene before parametrization. This extraction is divided in two main steps: the object segmentation and the labeling of the objects.

Object segmentation. The segmentation step consists in determining which of the discrete volume voxels belong to objects of interest or to the background. In order to obtain this segmentation we used a simple intensity threshold on the voxel values. This threshold was interactively chosen by the user using the display of orthogonal cross sections (*xy*, *yz*, and *xz*) of the discrete volume (Fig. 1). Thus, it was possible to visually assess the effect of the thresholding on the entire discrete volume.

Labeling. Once the object and background voxels were known, it was necessary to identify separate objects in the discrete volume. Therefore, the labeling process assigns the same label value to each connected voxel of an object. After this step, each separate object in the discrete volume can be recognized by its label value.

Our labeling algorithm is based on the extension of a simple 2D seed fill algorithm (15) to 3D space. In principle, the discrete volume is scanned linearly until a voxel belonging to the object class ("1" value) is encountered. From this voxel, the 3D seed fill algorithm is used to find and assign the current label value to all the connected object voxels. During this step, the programme requires a "Last In First Out" storage stack to store (PUSH) the coordinates of selected voxels and

to retrieve (POP) these coordinates. Then, the label value is incremented, and the scanning step resumes starting from the previous seed until a nonlabeled object voxel is found, or the end of the discrete volume is reached. While an object is being labeled the algorithm also computes its size. Thus, size filtering may be done: The user sets a size range in which objects are kept and labeled (objects outside this size range are eliminated). The labeling algorithm also excludes the cut objects (objects that share voxel(s) with the borders of the discrete volume). The labeling algorithm is described as follow:

```
FUNCTION FillObject(Object Voxel Index i, j, k;
Value Label)
  INITIALIZE the stack;
  Set CounterSize to 0;
  Set V(i, j, k) to Label;
  PUSH the Object Voxel Index (i, j, k) onto the stack;
  WHILE (the stack is not empty) DO
    POP Object Voxel Index (l, m, n) from the stack;
    Increment CounterSize;
    FOR (each of the 6-connected voxels (Vneig) adjacent to V(l, m, n)) DO
      IF NOT (Vneig equals background voxel OR
      Vneig equals Label) THEN
        PUSH Vneig Object Voxel Index onto the
        stack;
        Set Vneig to Label;
      ENDIF
    ENDFOR
    IF (the Stack is "full − 6voxels ObjectVoxel-
    Index") THEN
      FOR (each voxel V in the stack) DO
        IF (the 6-connected voxels adjacent to the V
        equal Label) THEN
          Remove the voxel V from the stack;
          Increment CounterSize;
        ENDIF
      ENDFOR
    ENDIF
  ENDWHILE
  Return CounterSize;
ENDFUNCTION.
FUNCTION LABELING
  Initialize BackGroundValue;
  IF (remove cut object) THEN
    FOR (all the voxel V of the border sides of the
    discrete volume) DO
      IF (V equals object voxel) THEN
        FillObject(V coorsdinates, BackGround-
        Value);
      ENDIF
    ENDFOR
  ENDIF
  set SizeThresholdDown to user's value;
  set SizeThresholdUp to user's value;
  set FillValue to FirstLabel;
  FOR (all the voxel V of the discrete volume) DO
    IF (V equals object voxel) THEN
      Set size to FillObject(V coorsdinates, FillValue);
      IF (size < SizeThresholdUp OR size > Size-
      ThresholdDown) THEN
        FillObject(V coorsdinates, BackGround-
        Value);
      ELSE
        Increment FillValue;
      ENDIF
    ENDIF
  ENDFOR
ENDFUNCTION
```

Once the objects are labeled in the discrete volume, the individual objects can be extracted from the discrete volume by thresholding the label values.

Distance encoding and morphological operations. In many applications of digital image analysis it is essential to measure the distance between elements (examples are texture description (16) and object shape description (17)). A distance transform converts a binary picture containing background and object elements to a distance map, where each element has a value that approximates the nearest distance to the element defined as the origin (reference set). For example, the border elements between background and object may be selected as the reference set. Thus, when the distance transform is completed, the border object voxels will have the smallest distance value (i.e., 1) and the centred voxels the greatest one. The voxels that are equidistant from the background (voxels with the same distance value) define a level surface inside the object. Each level surface may be compared to an "onion skin" that surrounds the level surfaces of greater distance value. Different kinds of distance transforms have been described and compared in the literature (18). The chamfer method was used in our application because this method leads to a good approximation of the distance in a short computing time (19).

For the sake of clarity, the chamfer algorithm will be first described in 2D space and then extended to the third dimension. Let Im be a 2D digitized image of N lines and M columns. The distance map is built in two steps (Fig. 2): the "forward pass" scans pixels from left to right and top to bottom; and the "backward pass" scans pixels from right to left and bottom to top. During each path, pixels with values different from the background value are searched. Each time one such pixel

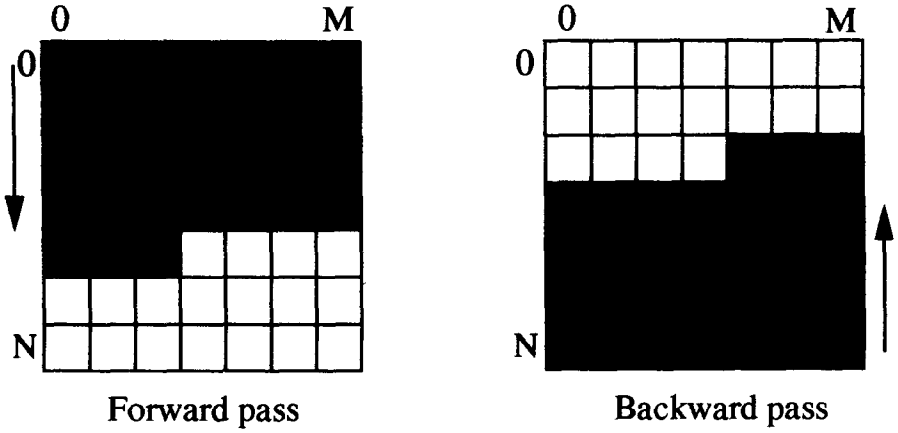

Fig. 2. The two passes of the chamfer algorithm in two-dimensions (2D). The forward pass goes pixelwise from left to right (0 to M) and linewise from top to bottom (0 to N); the backward pass follows the reverse path. The greyed pixels are already scanned pixels and the white ones are pixels that have not yet been scanned.

is found, pixel values of the already scanned neighbors (object and background pixels) are used to determine the value of the current pixel. Because neighbors may be lateral or diagonal, their physical distances from the current pixel are different, and this must enter in the calculation of the current pixel value. The chamfer method takes this difference into account by using additive masks (Fig. 3). The integer distances inside these masks approximate the physical distances multiplied by a scale factor: scale factor = 3; lateral length = 1 ($d1 = 3$); diagonal length = $\sqrt{2} \approx 4/3$ ($d2 = 4$). Values of already scanned pixels (distance values) are weighted by their corresponding mask values (physical distance of the scanned pixel to the current pixel) to determine the shortest distance from the background to the current pixel (Fig. 4). In the case of the backward path, this shortest distance value is compared to the current pixel value and the minimum value is kept. Because the distance $d1$ and $d2$ are approximated by 3 and 4, respectively, the distance map contains distance values scaled by a factor of 3. The actual distance of each pixel is obtained by dividing the distance value inside the map by 3.

The extension to the third dimension is straightforward: The forward path proceeds voxel by voxel from the right to the left, line by line from top to bottom, section by section from the first to the last. The size of the neighborhood is increased by the nine neighbors of the section above and the nine neighbors of the section below. Another distance is introduced leading to three different kinds of neighbors: those who share a corner at distance $d3 = \sqrt{3} \approx 9/5$; those who share a line at distance $d2 = \sqrt{2} \approx 7/5$; and those who share a facet at distance $d1 = 1 = 5/5$. Two masks are used for the different paths integrating the 3D neighborhood (Fig. 5). Because the scale factor is 5, the distance map is now divided by 5. The pseudocode of the distance transform is described as follow:

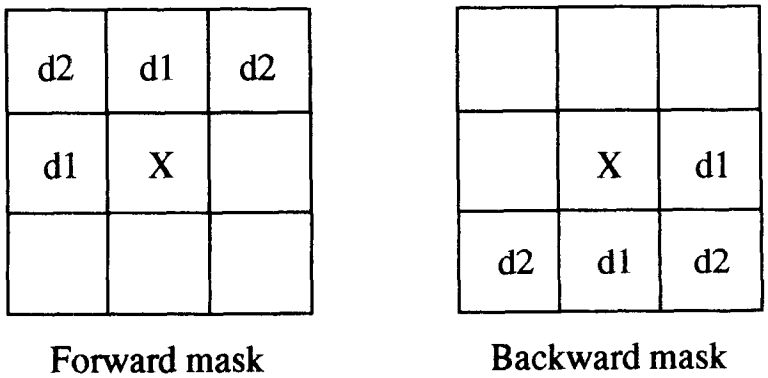

Fig. 3. Distance masks of the chamfer algorithm in two dimensions (2D). The masks include different distances $d1$ and $d2$. These are integer approximations: $\sqrt{2}$ can be approximated by the ratio 4/3, then $d2 = 4$ and $d1 = 3$. X represents the position of the current pixel and the empty spaces refer to the not yet scanned pixels (ignored).

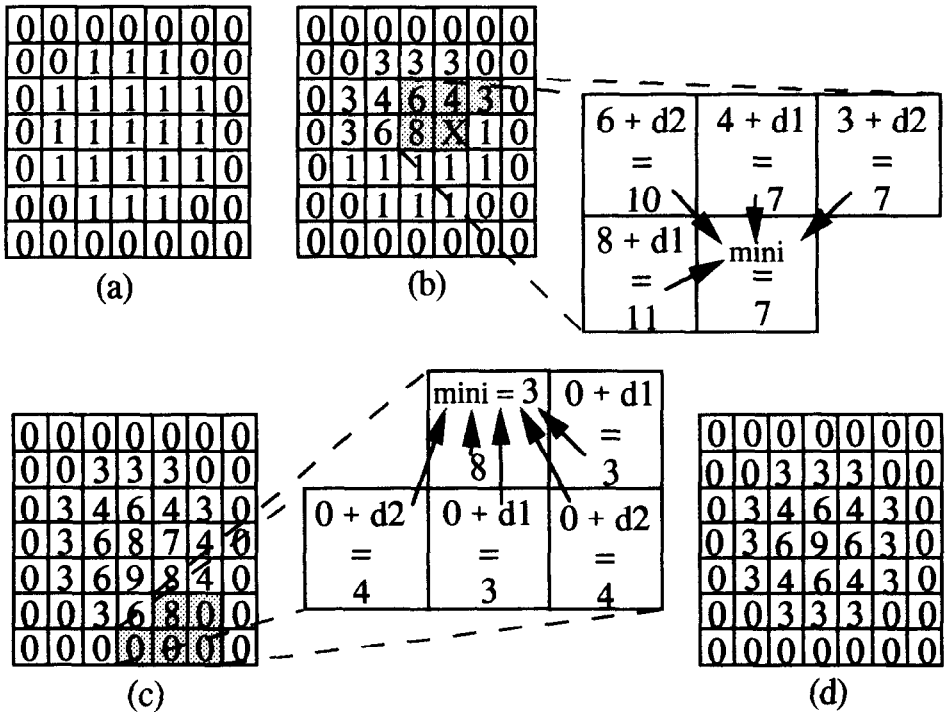

Fig. 4. Building of the distance map (2D). (a) Binary image; "0" values; background pixels; "1" values object pixels. (b) Processing of a point (X) during the forward path using the distance mask. (c) Result of the forward path and calculation of the first distance value by the backward path. (d) Distance map at the end of the backward path processing.

Let V be a discrete binary volume made of Z sections of L lines and M columns.

FUNCTION FindMinForward(m, l, z)
  Value = $min(V(m-1, l-1, k-1) + d3, V(m, l-1, k-1) + d2, \ldots, V(m-1, l, k) + d1)$;
  return Value;
END FUNCTION
FUNCTION FindMinBackward(m, l, z)
  Value = $min(V(m+1, l+1, k+1) + d3, V(m, l+1, k+1) + d2, \ldots, V(m+1, l, k) + d1)$;
  Value = min (Value, $V(m, l, z)$);
  return Value;
END FUNCTION

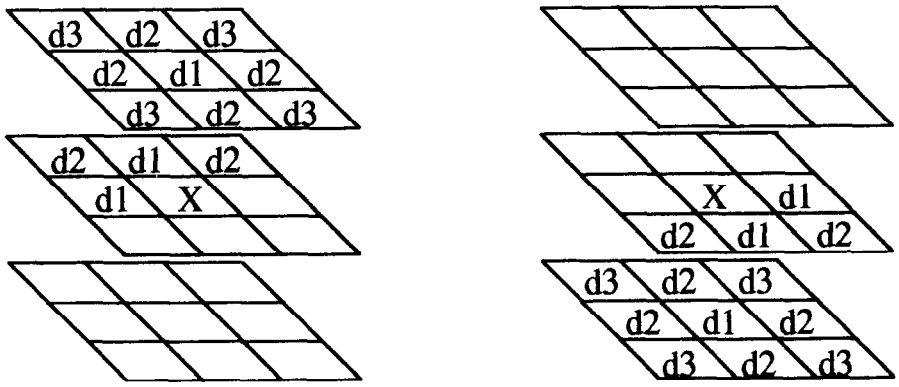

Fig. 5. Three-dimensional (3D) distance masks. $d1$, $d2$, and $d3$ are respectively set to 5, 7, and 9 (scale factor = 5). X represents the position of the current pixel and the empty spaces refer to the not yet scanned pixels (ignored).

```
FUNCTION DistanceMap()
  FOR z = 2 TO Z − 1 DO
    FOR l = 2 TO L − 1 DO
      FOR m = 2 TO M − 1 DO
        IF (v(m, l, z) > 0) THEN
          v(m, l, z) = FindMinForward(m, l, z);
        ENDIF
      ENDFOR
    ENDFOR
  ENDFOR
  FOR z = Z − 1 TO 1 DO
    FOR l = L − 1 TO 1 DO
      FOR m = M − 1 TO 1 DO
        IF (v(m, l, z) > 0) THEN
          v(m, l, z) =  FindMinBackward(m, l, z);
        ENDIF
      ENDFOR
    ENDFOR
  ENDFOR
  FOR (all the voxel v of the discrete volume) DO
    IF (v > 0) THEN
      v = v/5;
    ENDIF
  ENDFOR
ENDFUNCTION
```

Morphological operations may be implemented directly from the chamfer algorithm. These morphological operators are used to smooth object shape, or to separate connected object.

a) Shrinking. To shrink an object, first the distance map of the discrete volume is built. Then the size of the shrink operator is set by a threshold value applied on the distance map. The shrunken object is made of voxels having values greater than the threshold value.

b) Expanding. The expanding of an object is obtained by shrinking the background. A boolean NOT operator is used to transform the discrete volume. The shrunken volume of the new object (former background) is calculated as described above. Again, a NOT operator is applied to retrieve the actual expanded object.

c) Closing and opening. As in two dimensions, the opening operation results from a shrinking operation followed by an expanding operation. The closing operation results from an expanding operation followed by a shrinking operation.

Biological application

The distribution of DNA replication foci was determined quantitatively during the *S* phase of the normal fibroblastic human cell line MRC-5 (16). Conventional microscopic fluorescence images using 2D mathematical tools (20) were used. Because of the 2D projection, some of the replication patterns were insufficiently characterized in particular patterns of the end of the *S* phase showing both perinuclear and nucleoplasmic replication. This study was now extended to 3D. Therefore, we verified the ability of the 3D tools to retrieve the distribution of the replication foci in 3D nuclear volumes obtained using confocal laser scanning microscopy. Total DNA and DNA replication foci were stained as described previously (16). Briefly, total DNA was stained using propidium iodide (PI) and DNA replication foci were revealed after BrdUrd incorporation and indirect immunofluorescence (FITC-conjugated antibody). Fluorescent dyes were simultaneously excited at 488 nm with an Argon laser. The emission filter for FITC was a 515–545 nm bandpass; for PI, a dichroic filter of 580 nm was used combined with a 590 nm longpass filter. Each acquisition leads to a data set of two discrete volumes: the fluorescence intensity of PI is sampled into the "DNA discrete volume" (Ddv), and the fluorescence intensity of FITC is sampled into the "BrdUrd discrete volume" (Bdv). The following examples illustrate the accuracy of the above quantitative method.

The preprocessing tools described above were used to enhance data in the two discrete volumes Bdv and Ddv (Fig. 6). Then, the nuclear volume was extracted from the Ddv using the segmentation and labeling functions. The nuclear volume was smoothed using a closing operation. A distance map of the nuclear volume was obtained by the chamfer method. Thus, each voxel of the Ddv belonging to the segmented nuclear volume was defined by its distance from the nuclear border. The fluorescent spots inside the Bdv were extracted by a segmentation step. In this way, each voxel of the Bdv also belonging to the nuclear volume was defined in terms of object voxel (replication site voxel) and background voxel (BrdUrd unstained nuclear site voxel). For each level surface of the distance map (Ddv), the number of object voxels (Bdv) was counted and normalized by the total number of voxels in the level surface. This information was expressed as a histogram of the normalised number of object voxels (replication site voxels) according to the distance from the nuclear border. In addition, the size of each object (replication foci) was calculated from the Bdv by a labeling process.

RESULTS

Reconstructed stereo views of the Bdv show that the spatial distribution of the replication foci varies between different nuclei (Fig. 7). In the nucleus of the first part of the *S* phase, the replication foci are homogeneously distributed inside the nuclear volume,

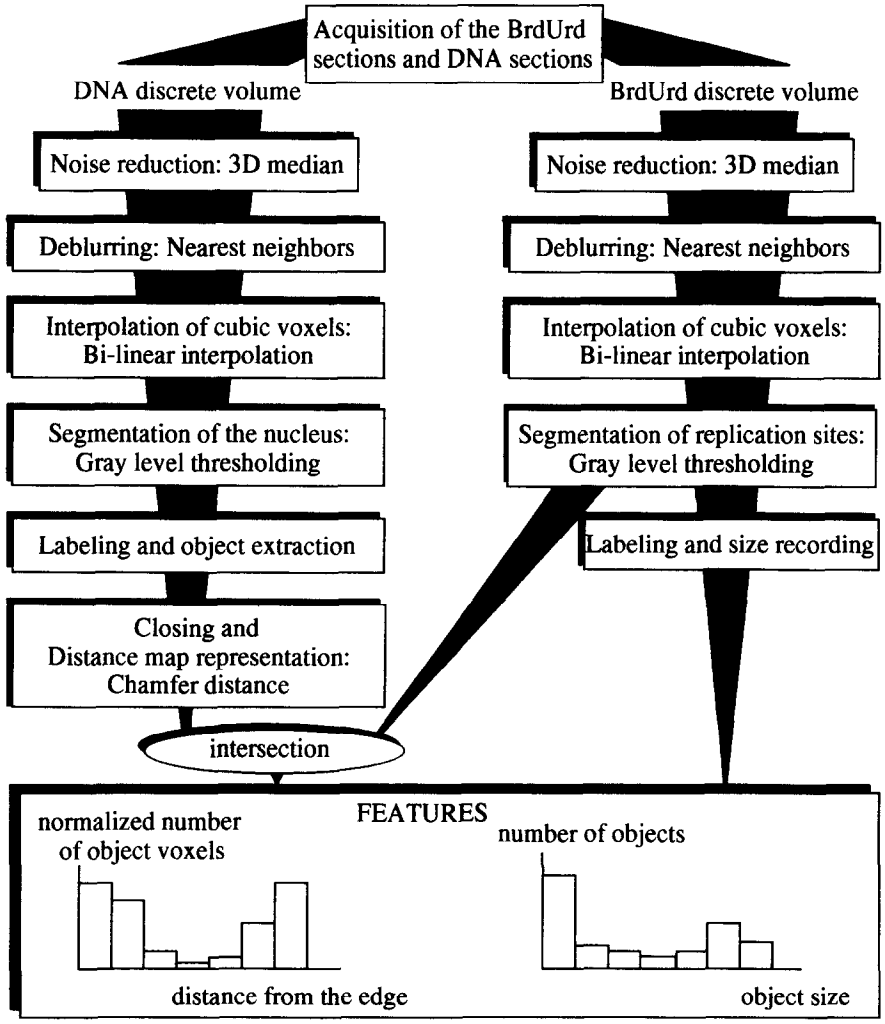

Fig. 6. Processing steps of the biological examples. This figure must be read by following the grayed lines.

and it is obvious that in the late *S* phase nucleus the replication distribution is rather perinuclear and perinucleolar. It may be also noted that the size of the replication foci varies, some being larger in the late *S* phase nucleus.

The programme of 3D quantitative analysis described above was applied to two examples. The quantitative topographical distribution is based on distance level encoding. The result of the level surface computation is shown in Fig. 8. In this process, each voxel in the nuclear volume is characterized by its distance to the nuclear border. The spatial distribution of the replication sites in the nuclear volume may now be represented by a frequency histogram of the distances from the nuclear border. Each frequency is weighted by the total number of voxels of the corresponding level surface (Fig. 9). The histogram of the late *S* phase nucleus retrieves the spatial distribution of the replication previously observed in the stereo view (Fig. 7). Indeed, the segmented replication foci are mainly distributed in the peripheral level surface and in the centered level surfaces. In the second case (nucleus of the first part of *S* phase), the frequency of the segmented replication foci gradually increases from the peripheral level surface to the centred level surfaces. This result differs from the spatial homogeneity visually observed in the stereo view. This difference can be explained by the ray tracer method used to obtain the stereo views: The intensity of each pixel in the stereo view is the result of voxel intensity integration (transparency rendering) along each ray through the discrete volume. If no discontinuity is encountered in the gray level distribution, the integrated result of a gradient will look homogeneous. This shows that although 3D reconstructions are very helpful to understand a 3D structure, a quantitative analysis must also be performed to avoid visual bias.

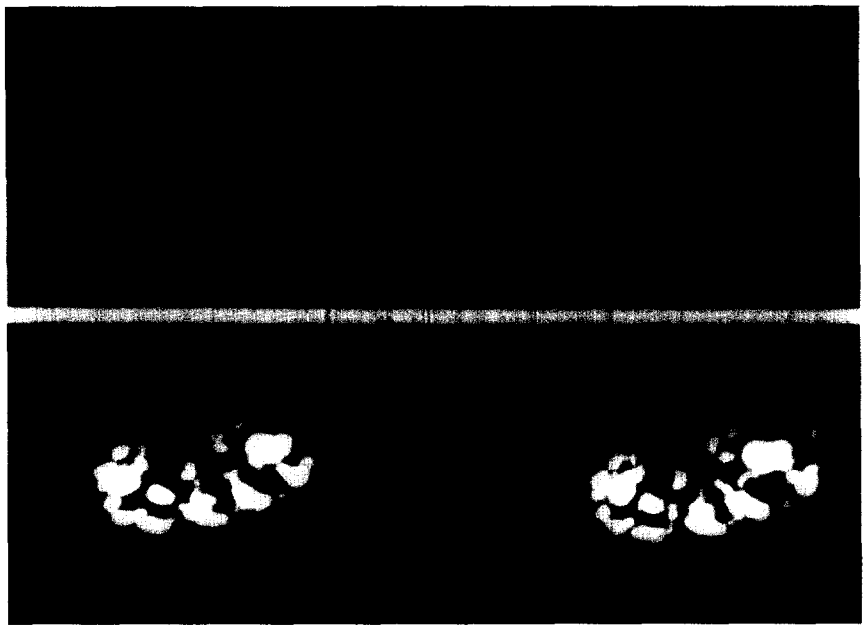

Fig. 7. Stereo views of BrdUrd stained nuclei. The stereo views are obtained using conventional ray tracer and transparency model. The top nucleus belongs to the first part of *S* phase (the fluorescent foci seem to be homogeneously distributed in the nucleus). The bottom nucleus is a late *S* phase one (the fluorescent foci distribution is rather perinuclear and perinucleolar).

Intranuclear labeling of the replication foci was used to estimate their size (number of voxels) and number. Figure 10 shows the frequency histograms of the replication focus sizes. It can be observed in both nuclei that many small foci are present. The largest replication foci are found in the late *S* phase nucleus. As an extension of the method, it would be of interest to combine the size and the localization

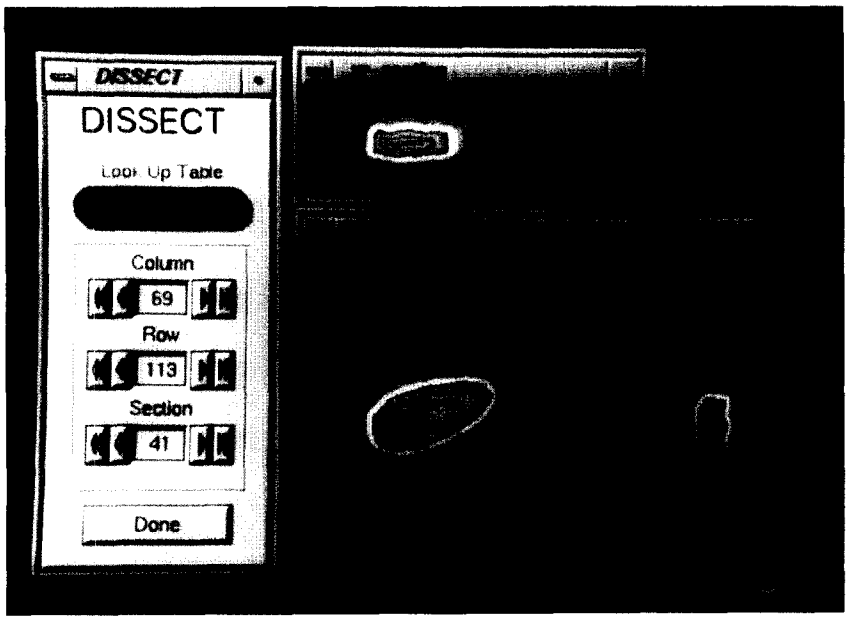

Fig. 8. Level surfaces. The result of the level surfaces is shown on *xy*, *xz*, and *yz* orthogonal cross sections. Each grey level represents a level surface. The user may verify the coherence of these surfaces through the entire discrete volume using the dialogue box options.

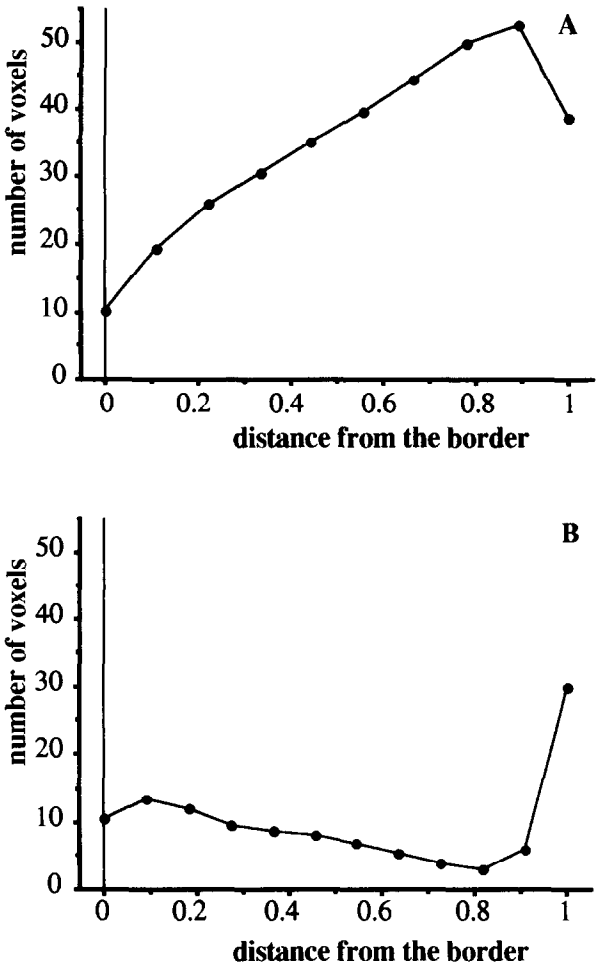

Fig. 9. Distribution of the BrdUrd-stained sites. Number of object voxels (BrdUrd-stained) per level surface. The number of level surfaces is normalized. Thus, the shortest distance from the border of the nucleus is 0 and the greatest one is 1. The number of object voxels was normalized by the size of the level surface. (A) Nucleus at the first part of the *S* phase; gradual increase of the number of replication sites from the periphery to the center. (B) Late *S* phase nucleus; replication sites are mainly distributed at the periphery and at the center.

information in order to study the relationship between the size and location of the replication foci, and whether different foci are associated with a particular structure in the nucleus (i.e., chromatin condensation states, nucleoli, etc.).

The computing times of the different parts of the analysis are summarized in Table 1. The total analysis time of about 10 min is short enough to allow a statistical analysis of a set of cell nuclei. In addition, the labeling algorithm takes 45 s for 256 × 256 × 72 voxels. Although it is difficult to compare computing times for such algorithms because they are directly dependent on the content of the volume data sets (size and shape of the objects), this time is shorter than the time spent by algorithms using a reorganization of a label table and a systematic scanning of the volume (21): 2.3 min for 512 × 512 × 8 voxels.

In conclusion, the different tools were proved to be efficient in the quantitative description of intravolumic events in the biological examples. It is thus possible to use these tools for the 3D quantitative description of the DNA replication throughout the *S* phase. The various tools we present in this paper, can be considered as the basic tools of a 3D biological image analyzer: The preprocessing tools can be used for general purpose 3D image enhancement, and the processing tools offer features that can be used to segment and analyze the morphology and the topography of 3D biological structures. All these tools are therefore applicable to many other biological applications, such as studying the intranuclear localizations of genes or to study the distribution of cells in a tissue.

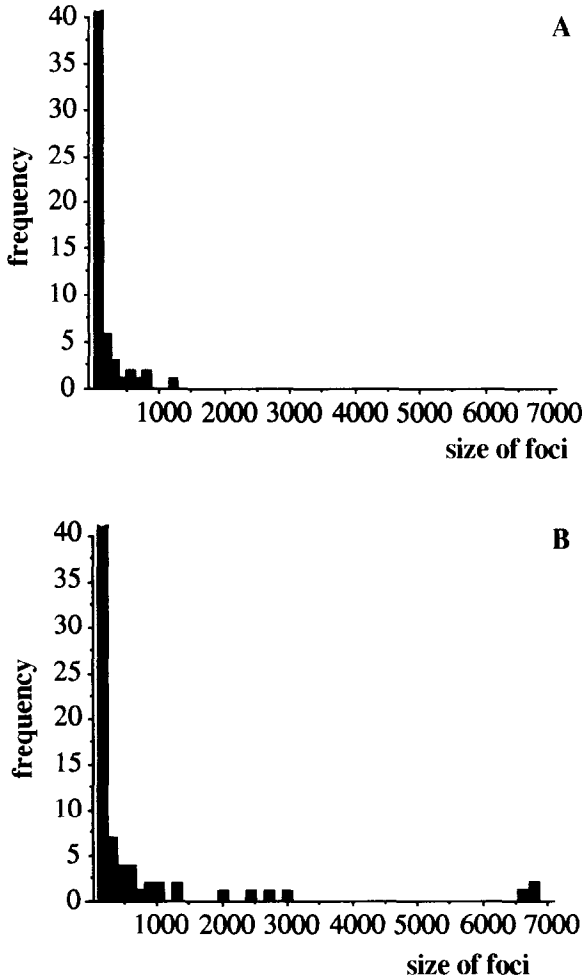

Fig. 10. Size of replication foci. The histograms show the distribution of the segmented foci as a function of their size. (A) nucleus of the first part of the *S* phase. (B) late *S* phase nucleus.

Table 1. Processing time of the presented tools

Name of the process	Size of data (in voxels)	Computing time	Comments
Median filter	256 × 256 × 39	25 s	
Debluring	256 × 256 × 39	38 s	
Interpolation	256 × 256 × 39 to 256 × 256 × 72	16 s	
Segmentation	256 × 256 × 72	3 s	Depending on the number and on the size of the object in the volume
Labeling	256 × 256 × 72	15–45 s	
Distance map	256 × 256 × 72	20–75 s	Depending on the size of the object in the volume
Biological example processing	2 volumes of 256 × 256 × 40 at the beginning of the process	≈10 min	Depending on the user interactions and on the size of the discrete volume

SUMMARY

The introduction of the CLSM makes it possible to acquire fluorescent specimens in 3D. We propose a method for the quantitative description of the 3D spatial distribution of events inside near-convex volumes. Considering the needs and the constraints in cellular biology, the computing time was one of our main considerations for the choice of specific tools. Two groups of tools were therefore selected and adapted: preprocessing and processing. All the tools are described in detail and algorithms are provided.

Preprocessing tools were used to restore and enhance the volume data, because the acquisition system generates artifacts that have to be corrected before any quantitative analysis. The high noise level was lowered using a 3D median filter; the out-of-focus blur was attenuated using the nearest neighbors method; and the cubic voxels were interpolated by the bi-linear approach.

Processing tools were then used to extract the significant objects from the volume and to compute intravolume distances or other features in order to quantify spatial information. The extraction of objects consists of an object segmentation step followed by an object labeling step. Segmentation was done by an intensity threshold on the voxel values, and our labeling algorithm was based on the extension of a simple 2D seed fill algorithm to 3D space. Size filtering and exclusion of cut objects were included in the labeling process. Intravolume distances were coded by level surfaces. The chamfer method was used for distance transforms. The size of neighborhood was 26 voxels, and the algorithm took into account the physical distances between neighbors who share a corner, those who share a line, and those who share a facet. Morphological operations (shrinking, expanding, closing, and opening) may be implemented directly from the chamfer algorithm. These morphological operators were used to smooth object shape, or to separate connected object.

These tools were applied to the description of the spatial distribution of DNA replication sites in mammalian cell nuclei as an example. The distribution was expressed in terms of normalized number of replication site voxels according to the distance from the nuclear border. In addition, the size of replication foci was calculated after a second step of labeling. The total analysis time of about 10 min is short enough to allow a statistical analysis of a set of nuclear cells and the various tools we present in this paper can be considered as the basic tools of a 3D biological image analyzer.

Acknowledgments—The authors wish to thank Dr. Mark Overmars (markov@cs.ruu.nl) for providing graphical user interface builder, Dr. Thérèse Ternynck for providing the BrdUrd monoclonal antibody. We are grateful to Edouard Thiel, Etienne Bertin and Raphaël Marcelpoil from our laboratory for helpful discussions during this work and to Dr. Victoria von Hagen for her advice in editing of the manuscript. This work was supported by the European Economic Community (GENO-CT91-0029).

REFERENCES

1. Van Der Vort, H.T.M.; Brakenhoff, G.J.; Baarslag, M.W. Three-dimensional visualization methods for confocal microscopy. J. Microsc. 153(2):123–132; 1989.
2. Forsgren, P.O. Visualization and coding in three-dimensional image processing. J. Microsc. 159(2):195–202; 1990.
3. Shotton, M.S. Confocal scanning optical microscopy and its applications for biological specimens. J. Cell Sci. 94:175–206; 1989.
4. Barillot, C.; et al. Computer graphics in medicine: A survey. CRC Critical Reviews in Biomedical Engineering. Boca Raton, FL: CRC Press; 1988 15(4):269–307.
5. Herman, G.T. A survey of 3D medical imaging technologies. IEEE Eng. Med. Biol. 9(4):15–17; 1990.
6. Sabri, M. Filtrage et restauration en traitement des images numériques: recherche d'une mise en œuvre automatique. France: University of Rennes I; 1991. Thesis.
7. Shaw, P.J.; Rawlins, D.J. Three-dimensional fluorescence microscopy. Prog. Biophys. Mol. Biol. 56:187–213; 1991.
8. Rolland, F.; Montanvert A. Graph matching for 3D reconstruction from cross-sections using simulated annealing. In: Johansen, P.; Olsen, S., eds. Proceedings of the 7th Scandinavian Conference on Image Analysis. Aalborg, Denmark: Pattern Recognition Society of Denmark; 1991:395–402.
9. Shaw, J.P.; Rawlins, D.J. The point-spread function of a confocal microscope: Its measurement and use in deconvolution of 3-D data. J. Microsc. 163:151–165; 1991.

10. Agard, D.A.; Hiraoka, Y.; Sedat, W.J. Three-dimensional microscopy: Image processing for high resolution subcellular imaging. SPIE 1161:24–30; 1989.
11. Carrington, W.A.; Fogarty, K.E.; Fay, F.S. 3D fluorescence imaging of single cells using image restoration. In: Foskett, J.K.; Grinstein, S., eds. Noninvasive techniques in cell biology. New York: Wiley-Liss; 1990: 53–72.
12. Conchello, J.A.; Hansen, E.W. Enhanced 3-D reconstruction from confocal scanning microscope images. 1: Deterministic and maximum likelihood reconstructions. Appl. Opt. 29(26):3795–3804; 1990.
13. Agard, D.A.; et al. Fluorescence microscopy in three dimensions. In: Taylor, D.L.; Wang, Y.L., eds. Fluorescence microscopy of living cells in culture (part B). San Diego: Academic Press; 1989: 353–377.
14. Harrington, S. Computer graphics a programming approach. New York: McGraw-Hill; 1983.
15. Rogers, D.F. Procedural elements for computer graphics. New York: McGraw-Hill; 1985.
16. Humbert, C.; Usson, Y. Eukaryotic DNA replication is a topographycal ordered process. Cytometry 13(6):603–614; 1992.
17. Thiel, E.; Montanvert, A. Shape splitting from medial line using the 3–4 chamfer distance. In: Arcelli, C.; Sanniti di Baja, G.; Cordella, L., eds., VISUAL FORM: Analysis and recognition. Proceedings of the First International Workshop on Visual Form. Capri, Italy, 1991. New York: Plenum Press; 1992: 443–450.
18. Borgefors, G. Distance transformations in arbitrary dimensions. Comput. Vision Graph. Imaging Proc. 27:321–345; 1984.
19. Chassery, J.M.; Montanvert, A. Géométrie discrète en analyse d'images. Paris: Hermes; 1991.
20. Usson, Y.; Humbert, C. Methods for topographical analysis of intra-nuclear BrdUrd-tagged fluorescence. Cytometry 13(6):592–602; 1992.
21. Baumann, P.H.; Schormann, T.; Jovin, M.J. Three-dimensional component labeling of digital confocal microscope images enumerates replication centers in BrdUrd labeled fibroblasts. Cytometry 13:220–229; 1992.

About the Author—FRANCK PARAZZA received his degree in electronic engineering in 1987. He completed his M.S. in biomedical engineering at Joseph Fourier Université, Grenoble, France, in 1989 and is now completing research for a Ph.D. at Joseph Fourier Université on analysis of 3D confocal microscopy data.

About the Author—CATHERINE HUMBERT received her Ph.D. degree in cellular and molecular biology from Joseph Fourier Université, Grenoble, France, in 1992. At present, she is a research and teaching assistant in Biology at Joseph Fourier Université. Her research interest lies in eukaryotic DNA replication.

About the Author—YVES USSON received his Ph.D. degree in Cellular and Molecular Biology from the University Joseph Fourier, Grenoble, France, in 1985. In 1986, he was postdoctoral fellow of the University of Otago, New Zealand, in the department of physiology of the Medical School. In 1987, he served as a Research Assistant in Biology at the Joseph Fourier Université and is now a senior researcher of the Centre National de la Recherche Scientifique. His research interest lies in confocal microscope image analysis and cellular sociology and he is a member of the French Circle of Quantitative Microscopy and of the European Society for Analytical Cellular Pathology.